ACS OMEGA

http://pubs.acs.org/journal/acsodf

Article

# Enhancing Photocatalytic Efficiency of Spent Tea Leaf Powder on $ZnIn_2S_4$ Incorporation: Role of Surface Charge on Dye Degradation

Mool Chand, Swapnil Barthwal, Arun Singh Rawat, Manika Khanuja,* and Seema Rawat

Cite This: *ACS Omega* 2023, 8, 17880−17890

Read Online

ACCESS | Metrics & More | Article Recommendations

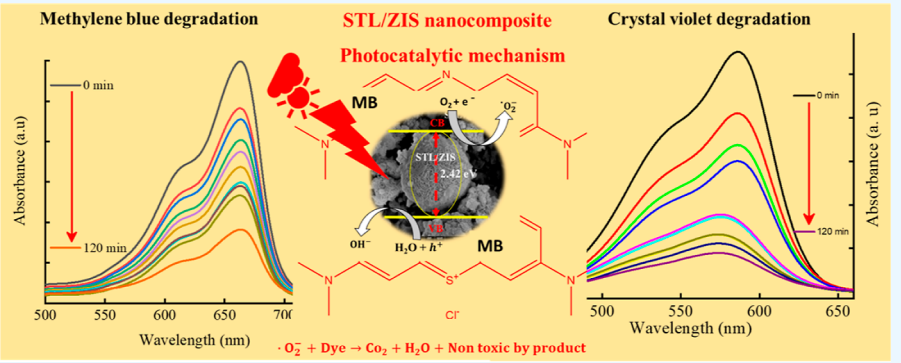


**ABSTRACT:** Photocatalytic degradation of dye contaminants using nanocomposite adsorbents has emerged as a promising solution for wastewater treatment. Owing to its abundant availability, eco-friendly composition, biocompatibility, and strong adsorption activity, spent tea leaf (STL) powder has been extensively explored as a viable dye-adsorbent material. In this work, we report spectacular enhancement in the dye-degradation properties of STL powder on incorporation of $ZnIn_2S_4$ (ZIS). The STL/ZIS composite was synthesized using a novel, benign, and scalable aqueous chemical solution method. Comparative degradation and reaction kinetics studies were performed onto an anionic dye, Congo red (CR), and two cationic dyes, Methylene blue (MB) and Crystal violet (CV). The degradation efficiencies of CR, MB, and CV dyes were obtained to be 77.18, 91.29, and 85.36%, respectively, using the STL/ZIS (30%) composite sample after the 120 min experiment. The spectacular improvement in the degradation efficiency of the composite was attributed to its slower charge transfer resistance (as concluded by the EIS study) and optimized surface charge (as concluded by $\zeta$ potential study). Scavenger tests and reusability tests deciphered the active species ($^{\bullet}O_2^-$) and reusability of the composite samples, respectively. To the best of our knowledge, this is the first report to demonstrate improvement in the degradation efficiency of STL powder on ZIS incorporation.

## 1. INTRODUCTION

Available freshwater amounts to less than 0.5% of all the water on earth, while its global consumption is doubling every 20 years.[1−3] To ensure perpetuated water supply, wastewater must be recycled. Organic (synthetic) dyes are integral components of wastewater, and these materials have low biodegradability and cause contamination of the land and water bodies.[4−6] Weathering of organic dyes via oxidation, hydrolysis, and other chemical reactions (occurring in the wastewater phase) generates toxic metabolites that impart adverse effects on the biological system.[7,8] Dye molecules are carcinogenic and hazardous to human health and marine organisms, even at low concentrations. Allergic dermatitis, skin allergy, and dysfunction of the sex organs, kidney, brain, liver, and so forth are caused by toxic dye molecules.[9−13] Advanced heterogeneous photocatalysis, employing semiconductor photocatalysts is a promising technology to degrade these contaminants. Semiconductor-mediated photocatalysis is an emerging sustainable technology, utilizing the solar insolation to activate the chemical reactions occurring at the surface of semiconductor catalysts.[14−16] This technique mineralizes a broad range of organic dyes into harmless byproducts such as $CO_2$, $H_2O$, and inorganic ions.[17−20]

Tea is the second most consumed beverage in the world, only behind water. Spent tea leaves (STLs) are therefore available as an abundant solid waste.[21,22] This material has been widely explored as a non-conventional and inexpensive adsorbent for the water contaminants (such as synthetic dyes), arsenic,

Received: February 13, 2023
Accepted: March 21, 2023
Published: May 12, 2023

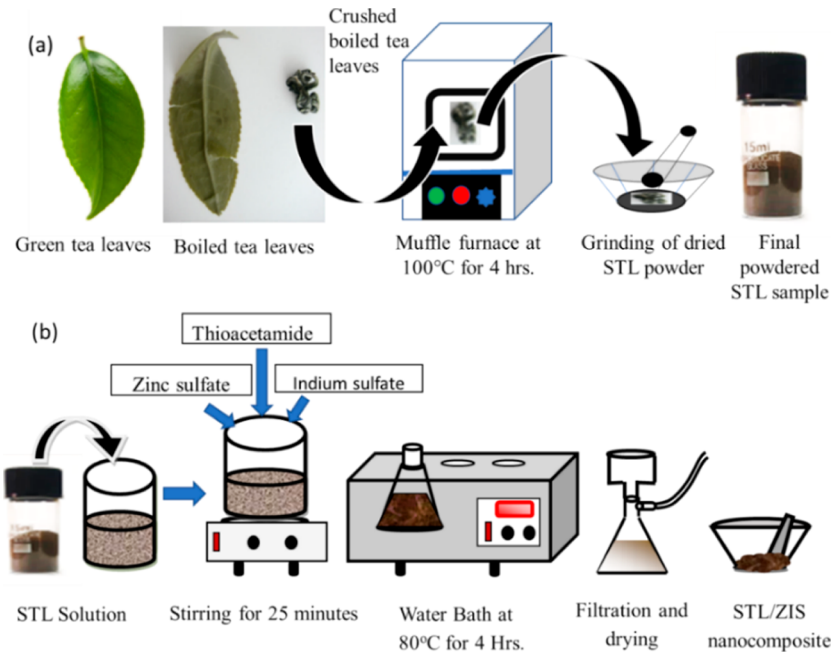


**Figure 1.** Schematic of synthesis route for the synthesis of (a) STL powder and (b) STL/ZIS composite.

cadmium, and lead.[21,23−30] Untreated STL usually exhibit very low removal efficiencies (<10%). Thermal activation of STL (200 to 400 °C, for up to 2 h) is generally required for significant improvement in removal efficiencies (>80%). Alternate ways to improve catalytic efficiency of STL is either via chemical modification using surfactants (such as polyethyleneimine)[31] or forming nanocomposites (such as with $CuFe_2O_4$).[32] Compared to metal oxides, metal sulfides exhibit narrower band gap, better suited for solar light harvesting. Ternary metal sulfides, for example, $ZnIn_2S_4$ (ZIS) have become a hotspot in the field of photocatalysis due to their strong resistance to photochemical corrosion and high photocatalytic efficiencies. Hexagonal ZIS has emerged as one of the leading photocatalyst, exhibiting high photocatalytic efficiency in various types of wastewaters.[33−36] In this study, the STL/ZIS composite was synthesized using a novel, cost-effective, aqueous chemical solution method at ambient temperature and pressures. We investigated comparative degradation of cationic and anionic dyes using STL/ZIS composite (with 0, 10, 20, and 30% ZIS incorporation). To the best of our knowledge, this is the first work to report the synthesis and study photocatalytic performance of STL/ZIS composite samples.

## 2. MATERIALS AND METHODS

**2.1. Materials.** The green tea leaves (Camellia sinensis) were purchased from Shaanxi Park Road Tea Co. Ltd., China. Hydrated zinc sulfate ($ZnSO_4{\cdot}7H_2O$ AR, 99.0%) and potassium iodide (KI AR, 99.0%) were purchased from Pallav Chemicals & Solvents Pvt. Ltd. Indium sulfate [$In_2(So_4)_3$ AR, 99.0%], thioacetamide ($C_2H_5NS$ AR, 98.0%), *t*-butanol [$(CH_3)_3COH$ AR, 99.0%], and congo red (CR) ($C_{32}H_{22}N_6Na_2O_6S_2$) were procured from Central Durg House (P) Ltd. Methylene blue (MB) ($C_{16}H_{18}N_3SCl$) and crystal violet (CV) dye ($C_{25}N_3H_{30}Cl$) were purchased from Thermo Fisher Scientific and Rankem brand chemical, respectively. *p*-Benzoquinone ($C_6H_8O_2$ AR, 99.0%) was supplied by Molychem Pvt. Ltd.

**2.2. Synthesis of STL Powder.** To synthesize STL powder, STLs were first washed with deionized (DI) water. The cleansed leaves were then dispersed in a boiling DI water bath and kept at 80 °C. Once the leaves turn colorless (after 4−5 h), these were airlifted from the bath using a tweezer and subsequently dried for 4 h in a muffle furnace at 100 °C. The dried STLs were then crushed and grinded using a mortar pestle, leading to a light brown powdered sample. Figure 1a shows the schematic of the STL powder synthesis route.

**2.3. Synthesis of STL/ZIS Composite.** To synthesize STL/ZIS composite samples, we have used the aqueous chemical solution method, schematically shown in Figure 1b. In this method, first, 500 mg of STL powder was dissolved in 50 mL of DI water. ZIS was synthesized using the synthesis route adopted in our previous study.[36] Zinc sulfate (4 mmol), indium sulfate (4 mmol), and thioacetamide (20 mmol) were dissolved in 80 mL of DI water and stirred for 10 min. In next step, STL powder solution is added to ZIS solution and stirred for 30 min. The final solution was transferred to a 250 mL conical flax and put in a water-bath at 80 °C. After 4 h, the final solution was cooled down to ambient temperature and the solution was filtered using a filtration unit. The residue was washed thoroughly with ethanol, followed by DI water. The residue was then dried in muffle furnace at 60 °C for 6 h and then grinded with mortar and pestle. Finally, a light yellow-brown colored powder [STL/ZIS (10%)] was obtained, which was used in further characterization and photocatalysis study. Other samples STL/ZIS (20%) and STL/ZIS (30%) were prepared by fine-adjusting the quantity of zinc sulfate, indium sulfate, and thioacetamide into the solution.

## 3. CHARACTERIZATION

**3.1. Material Characterization.** X-ray diffraction (XRD) system (Rigaku smart lab) was used for investigating the crystallinity in the STL/ZIS composite samples. Monochromatic Cu−$K_a$ (1.54 Å) was used for probing the samples, under applied 40 kV voltage and 40 mA current. The XRD was performed in Bragg−Brentano geometry ($\theta$−$2\theta$ mode) and the pattern was recorded at 0.02° $s^{-1}$. The field emission scanning electron microscopy (FESEM) technique [Quanta 3D FEG (FEI)] was used to determine the morphology of the powdered


https://doi.org/10.1021/acsomega.3c00955
ACS Omega 2023, 8, 17880−17890

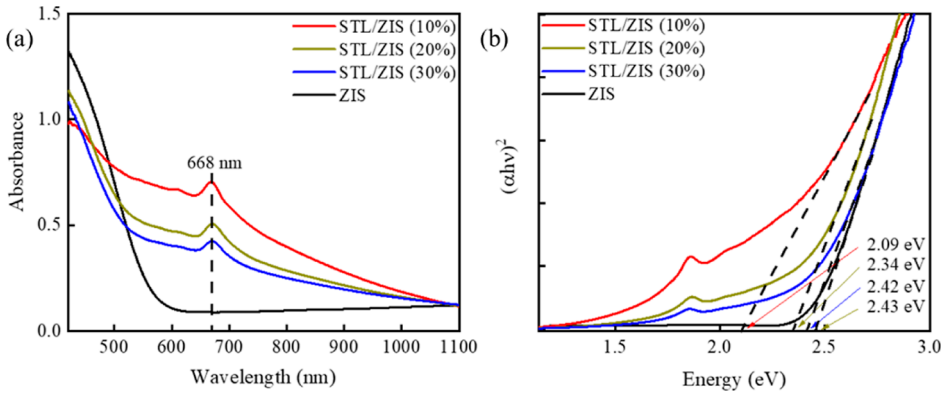


**Figure 2.** (a) UV−vis absorbance spectra and (b) Tauc's plots of STL/ZIS composites.

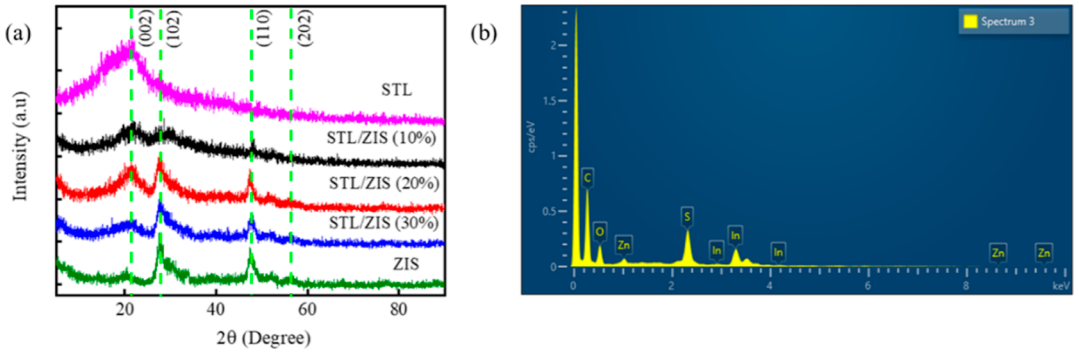


**Figure 3.** (a) XRD diffractogram and (b) EDX spectrum of STL/ZIS composites.

composite samples. Fourier transform infrared (FTIR) spectroscopy study was performed using Vertex 70 V, Bruker spectrometer. The IR absorption/transmission spectrum is crucial in identification of the functional groups and bond structure in molecules. The $\zeta$ potential of the composite sample was determined using Zetasizer Ver. 7.12 (MAL1192921) from Malvern Instruments. Electrochemical impedance spectroscopy (EIS) was conducted using a Metrohm Potentiostat/Galvanostat with a 1 M $Na_2SO_4$ electrolyte. The surface properties of the composite were analyzed using X-ray photoelectron spectroscopy (XPS) with a Thermo Scientific NEXA surface analyzer. The optical properties were analyzed using UV−visible (UV−vis) spectroscopy (Agilent Technology Cary 100 series).

**3.2. Photocatalytic Studies.** A comparative photocatalytic study of both anionic (CR) and cationic (CV and MB) dyes were performed on the STL/ZIS composite under the Xenon lamp (AM 1.5 G, 100 mW/cm$^2$). Different amounts of sample (STL/ZIS) were taken in the experiment to evaluate the degradation study. 1 mg of anionic dye (CR) and cationic dye (MG and CV) were dissolved in 100 mL of DI separately. To investigate the adsorption and photocatalysis study of the composite, the dye solution was placed in the presence and absence of the light source. To examine dye concentration, 1 mL of dye solution was taken out every 10 min (for the first hour) and every 15 min (in the next hour). The samples were analyzed using a UV−vis spectrophotometer at absorbance wavelengths of 498, 664, and 586 nm for CR, MB, and CV dyes, respectively. The dye degradation efficiency ($\eta$) was calculated using eq 1.

$$\eta = \frac{(C - C_o)}{C_o} \times 100\% \quad (1)$$

$C_o$ represents the initial concentration of the dye solution, while $C$ represents the concentration of the dye solution at time $t$.

## 4. RESULTS AND DISCUSSION

**4.1. UV−Vis Studies.** The UV−vis absorption spectra and corresponding Tauc's plots of STL/ZIS composites are shown in Figure 2a,b, respectively. The UV−visible absorbance peak of composites was obtained around 668 nm, which lies in the visible region.

The band gap of the pure STL/ZIS composite was determined using eq 2.

$$(\alpha hv)^n = A(hv - E_g) \quad (2)$$

where $\alpha$ is the absorption coefficient, h$\upsilon$ is the photon energy, $E_g$ is the optical band gap, and $n$ = 2 for the (allowed) direct transaction.[37] The band gap values were obtained from the intercept of linear region of $(\alpha hv)^2$ curve on the energy (h$\upsilon$) axis. The (direct) band gap values calculated for STL/ZIS (10%), STL/ZIS (20%), and STL/ZIS (30%) composites are 2.09, 2.34, and 2.42 eV, respectively. Incorporating more ZIS into the STL matrix was found to extend the optical band gap (of composite) from 2.09 to 2.42 eV, approaching that of bulk ZIS.

**4.2. XRD and EDX Studies.** The XRD diffractogram of the STL powder, ZIS, and STL/ZIS composite samples are illustrated in Figure 3a. The XRD results confirm the existence of two distinct phases (STL and ZIS) in the composites. All the XRD patterns exhibit one common broad peak (~21.34°), indicating (002) planes and poor crystallinity in STL powdered samples.[38] The relative intensity of this peak was found to decrease with the increase in STL content in the composites. The XRD pattern of composite samples exhibit three additional peaks (~27.41, 47.33, and 58.02°), indexed as (102), (110), and


https://doi.org/10.1021/acsomega.3c00955
ACS Omega 2023, 8, 17880−17890

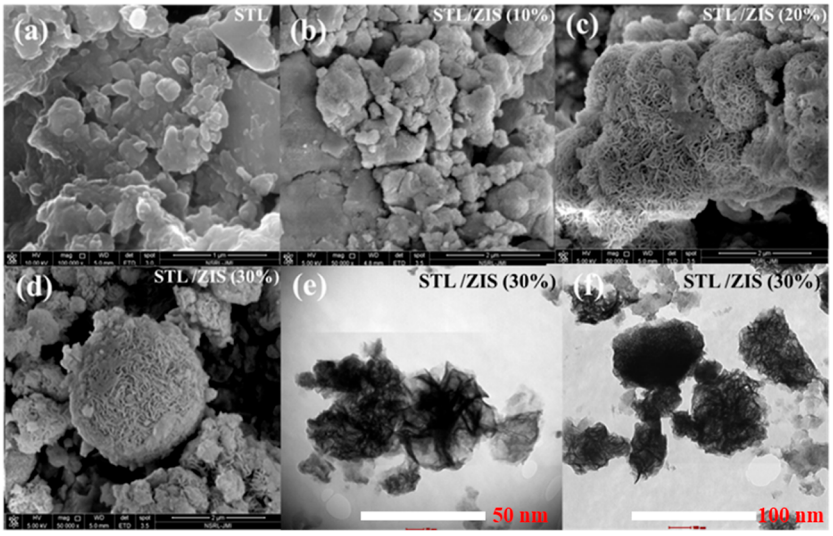


**Figure 4.** FESEM micrographs of (a) STL powder, (b) STL/ZIS (10%), (c) STL/ZIS (20%), (d) STL/ZIS (30%) composites, and HRTEM micrographs of STL/ZIS (30%) at different scales (e) 50 and (f) 100 nm, respectively.

(202) planes of (hexagonal) ZIS, respectively (JCPDS #03-065-2023).[36] EDX analysis was used to examine the chemical composition and purity of the as-synthesized STL/ZIS composite. Figure 3b displays an EDX spectrum that demonstrates the presence of zinc (Zn), indium (In), sulfur (S), carbon (C), and oxygen (O) within the composite sample. The spectrum clearly demonstrates that there are no impurities present in the composite sample. As a result, both XRD and EDX analysis demonstrate that the current synthetic method is effective in synthesizing the STL/ZIS composite.

**4.3. FESEM and HRTEM Studies.** The morphologies of the synthesized STL powder and the STL/ZIS composites were investigated using FESEM studies. The FESEM micrographs are presented in Figure 4a−d. Pristine STL powder exhibits a highly diversified and porous morphology.[38] The porous surface of the adsorbent provide a better medium for efficient adsorption of the dye molecules. On incorporating ZIS into STL matrix, the morphology becomes uniform, with apparent microspheres covering the whole surface. It is a well-known fact that the morphology of ZIS powder is typically dominated by the microspheres.[39] On raising the amount of ZIS from 10 to 30% STL/ZIS sample, these microspheres become distinctly more visible, confirming the existence of the ZIS phase. Figure 4e,f shows the HRTEM image of an STL/ZIS (30%) composite sample at two different scales (50 and 100 nm). The interaction between STL and ZIS was directly confirmed by two contrasted regions as shown in the HRTEM images. It can be clearly seen that the morphology of composite samples is dominated by uniformly distributed microspheres.

**4.4. FTIR Spectroscopy.** The chemical bonding and functional groups of the composite sample were examined using FTIR spectroscopy technique. FTIR spectrum of the STL/ZIS (10, 20, and 30%) composite was recorded in the range of 500−4000 $cm^{-1}$, as shown in Figure 5. The peak at 880 $cm^{-1}$ in the composite was assigned to the (out of plane) C−H bending in the benzene ring.[40] The peak centered at 1040 $cm^{-1}$ was attributed to the S═O bonds.[41] Peaks present at 1210, 1400, and 1610 $cm^{-1}$ corresponds to C−N, O−H, and C═C stretching, respectively.[42] Peaks corresponding to C═C═C, C≡C, and O═C═O bonds were centered at 2123 and 2329 $cm^{-1}$.[43] The peak at 2929 $cm^{-1}$ was assigned to the deformation

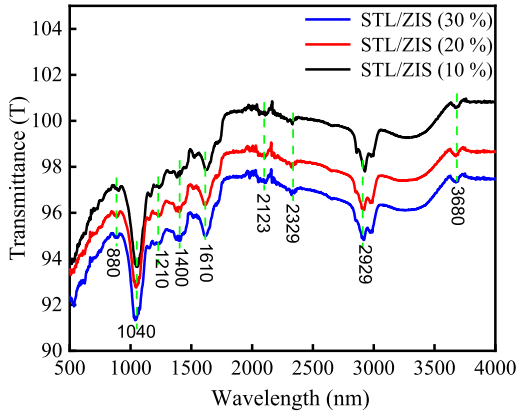


**Figure 5.** FTIR spectrum of STL/ZIS (10%), STL/ZIS (20%), and STL/ZIS (30%) composite samples.

vibration of the N−H group.[44] In addition, the peak at 3680 $cm^{-1}$ was attributed to the hydroxyl group (O−H) stretching vibration. FTIR spectrum suggests that our synthesized sample is devoid of impurity phases.

**4.5. X-ray Photoelectron Spectroscopy.** The oxidation state and elemental composition of the STL/ZIS (30%) composite sample was examined using XPS, as depicted in Figure 6a−f. The general XPS survey confirms the presence of Zn, In, S, C, and O element in the composite sample, as shown in Figure 6a. The core-level spectra of Zn (2p) are shown in Figure 6b. The binding energies of Zn (2p) cantered at 1021.2 and 1044.4 eV correspond to the $2p_{3/2}$ and $2p_{1/2}$ states, which shows that Zn exhibits the $Zn^{2+}$ oxidation state in the composite sample.[45] Figure 6c showed the core-level spectra of the In (3d) element. The binding energies of In ($3\ d_{5/2}$) and In ($3\ d_{3/2}$) are centered at 444.5 and 452.2 eV, respectively, and results confirmed that In exists in the $In^{3+}$ state.[46] Deconvolution of the S (2p) core-level spectra is shown in Figure 6d cantered at 161.4 and 162.7 eV into two separate peaks indexed as S ($2p_{3/2}$) and S ($2p_{1/2}$), confirming that S occurs in the $S^{2-}$ state[47] and extra peak at 164 eV indicates the sulfur oxidation. Figure 6e shows the carbon core-level spectra, and in spectra, three peaks are centered at 285.4, 286.9, and 287.4 eV corresponding to the C−



https://doi.org/10.1021/acsomega.3c00955
ACS Omega 2023, 8, 17880−17890

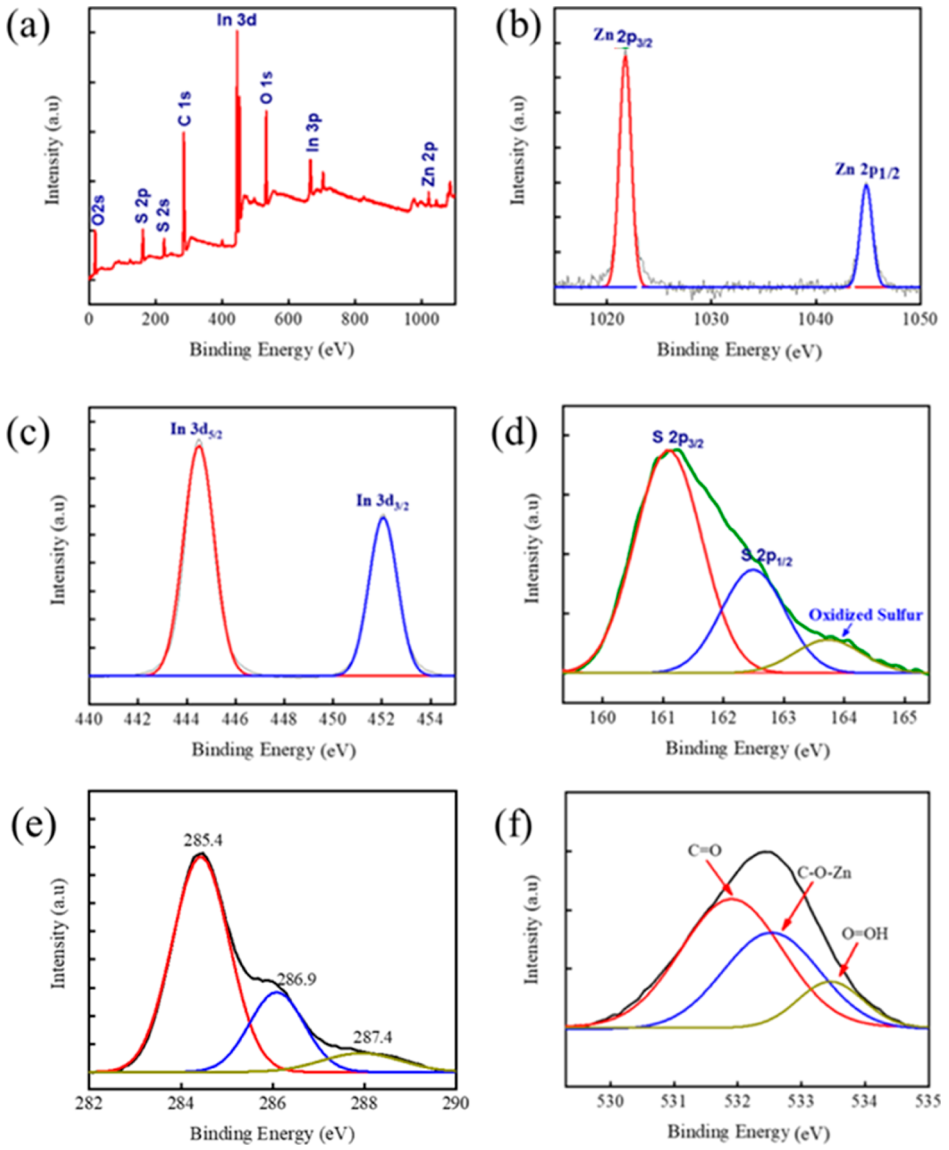


**Figure 6.** XPS study (a) survey scan and high-resolution core-level spectrum of (b) Zn 2p, (c) In 3d, (d) S 2p, (e) C 1s, and (f) O 1s of STL/ZIS (30%) composite.

OH/C−O−Zn, $Csp_2$, and C−H, respectively. In the oxygen core-level spectra, peaks located at 531.91, 532.26, and 533.8 eV correspond to the C═O, C−O−Mo, and O−OH bonds, as shown in Figure 6f. The XPS analysis result revealed the presence of various elements (Zn, In, and S) and their chemical states, which helped to understand the chemical composition and bonding behavior of the composite sample, and indicated that the STL/ZIS sample has a high purity and a well-defined chemical structure.

**4.6. Electrochemical Impedance Spectroscopy.** EIS study of the composite was carried out to better understand the impedance behavior of the composite sample. Nyquist plot of STL and STL/ZIS (10, 20, and 30%) composites sample is shown in Figure 7. According to Nyquist plot, the STL/ZIS (30%) composite has a small semicircular arc compared to the pure STL, STL/ZIS (10%), and STL/ZIS (20%) composite, indicating that it has low charge transfer resistance (Rct). Also, the EIS plot revealed that the slope of the STL/ZIS (30%) composite was significantly higher than that of the pure STL, STL/ZIS (10%), and STL/ZIS (20%) composite, indicating

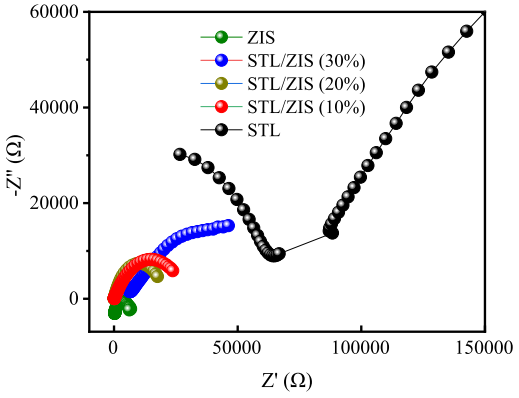


**Figure 7.** Electrochemical impedance plot of ZIS, STL, and STL/ZIS (10, 20, and 30%) composite samples.

that the material has a low diffusion resistance. Thus, the values of charge transfer resistance (Rct) for STL, STL/ZIS (10%), STL/ZIS (20%), STL/ZIS (30%), and ZIS were found to be


https://doi.org/10.1021/acsomega.3c00955
ACS Omega 2023, 8, 17880−17890

34253, 29733, 20894, 14814, and 10392 Ω. Thus, on incorporating ZIS into the STL matrix, the electron hole ($e^-$−$h^+$) pair separation rate was improved. The improved electron hole ($e^-$−$h^+$) pair separation rate was helpful for the photocatalytic degradation study of the composite.

**4.7. ζ Potential Study.** ζ potential study was performed on STL powder and composite samples in order to investigate the surface charge distribution, as depicted in Figure 8. An electric charge was formed on the dispersed molecules depending on the type of particle and its surroundings. There are two zones around the particle: an inner region (stern layer) and an outer region (diffused layer). The ζ potential is used to denote the potential difference between these two zones (inner region and outer region).[48] Surface charge plays an anchoring role during the interaction of the photocatalyst with the dye molecules.

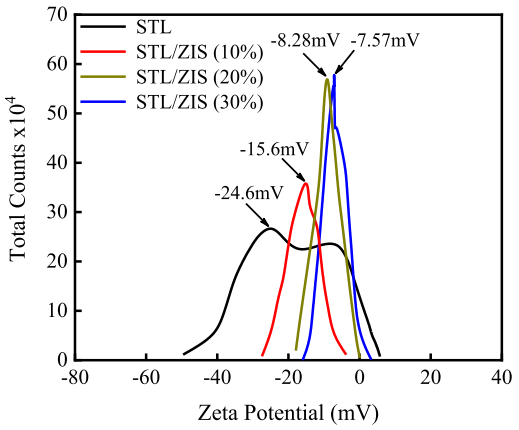


**Figure 8.** ζ potential plot STL and STL/ZIS (10, 20, and 30%) composites.

ζ potential study revealed that the STL surface was negatively charged with −24.6 mV, whereas the surface charge values of STL/ZIS (10%), STL/ZIS (20%), and STL/ZIS (30%) composites were −15.6, −8.28, and −7.57 mV, respectively. The negative surface charge on STL and composite surface is favorable for cationic (positively charge) dye adsorption due to hydrogen bonding and π−π interaction work in between amine and hydroxyl groups of dye and photocatalyst sample.[49]

In addition, the shifting of ζ potential (toward 0 eV) on ZIS incorporation also facilitates the adsorption of anionic dyes. The increase in the photocatalytic degradation efficiency of STL on incorporation of ZIS is due to the higher adsorption (via electrostatic interaction) of the negatively charged CR molecule. Electrostatics interaction is the strong interaction, dominates as compared to hydrogen bonding or π−π interaction in the CR molecule.[48] Thus, the degradation efficiency of STL increases on incorporation of ZIS, in the case of CR dye as will be discussed in the photocatalytic study.

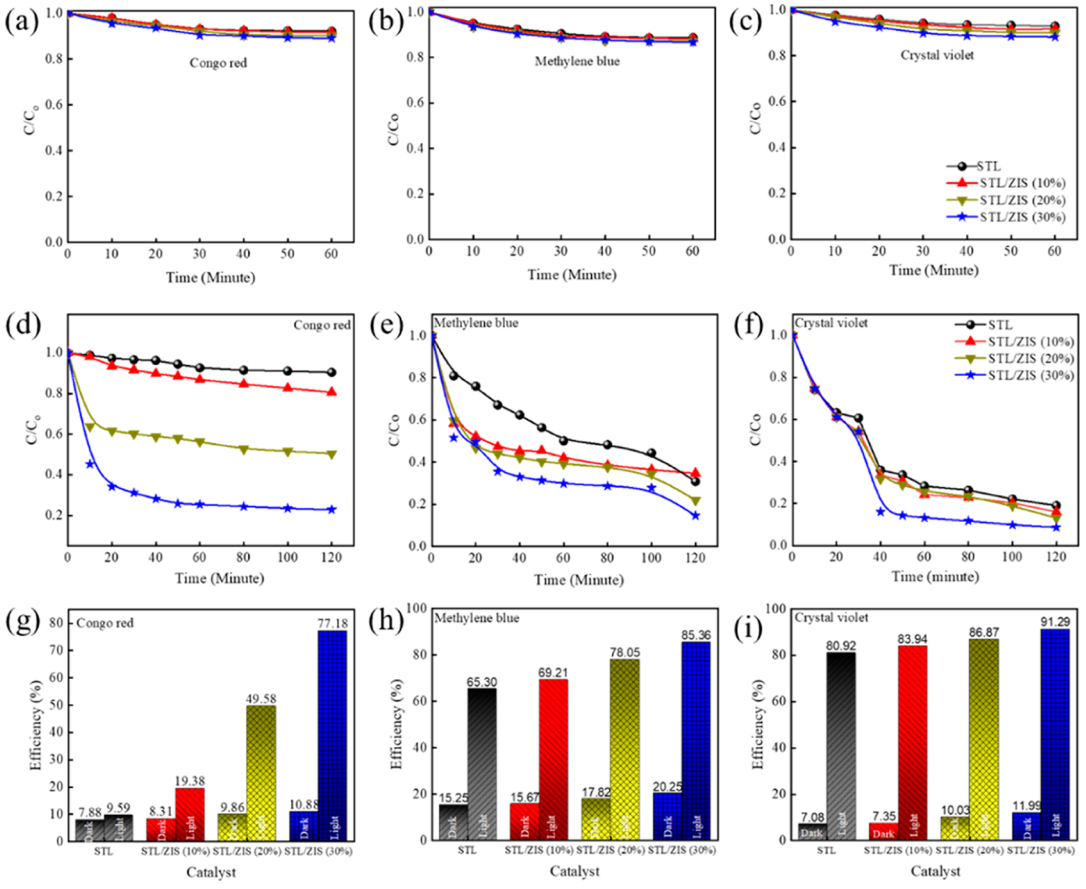


**Figure 9.** (a−f) $C/C_o$ vs time plots and (g−i) degradation efficiency ($\eta$) vs time plot for CR, CV, and MB dyes using STL/ZIS composite under the dark and light.



https://doi.org/10.1021/acsomega.3c00955
ACS Omega 2023, 8, 17880−17890

**Table 1. Previously Reported Dye Removal Study Using Different Agriculture Wastes, Explored as Low-Cost Adsorbents**

| agriculture waste | dyes | time duration | percentage removal (%) | references |
|---|---|---|---|---|
| banana bark, banana peel powder | basic violet 10, Rhodamine B | 40, 60 min | 85.0, 81.01 | 50, 61 |
| tamarind shell | CR | 4 h | 83.0 | 51 |
| neem leaf powder | CR | 5 h | 99.0 | 52 |
| rice husk | direct F. Scarlet, malachite green, and MB | 90, 40, 30 min | 80.0, 94.41, 95.0 | 53, 55, 56 |
| neem bark | malachite green | 7 h | 88.45 | 54 |
| mango bark | malachite green | 7 h | 99.45 | |
| wheat straw | basic yellow 21 | 48 h | 50.9 | 57 |
| mangrove bark | direct red-23 | 4 h | 90.0 | 58 |
| P. oceanica leaf | reactive red 23 | 10 h | 80.0 | 59 |
| teak tree bark | MB | 30 min | 97.0 | 60 |
| tapioca peel waste | rhodamine B | 120 min | 90.4 | 62 |
| pomegranate peels | rhodamine B | 10 min | 89.8 | 63 |
| STLs | reactive green 19; reactive violet 5, MB | 60, 60, 200 min | 98.8, 72.8, 98.0 | 64, 65 |
| STL modified with polyethyleneimine (PEI-STL) | reactive black 5 and methyl orange | 150 min | 97.59 | 31 |
| STL/ZIS composite | CR, MB, and CV | 120, 120, 120 min | 77.18, 85.36, 91.29 | present work |

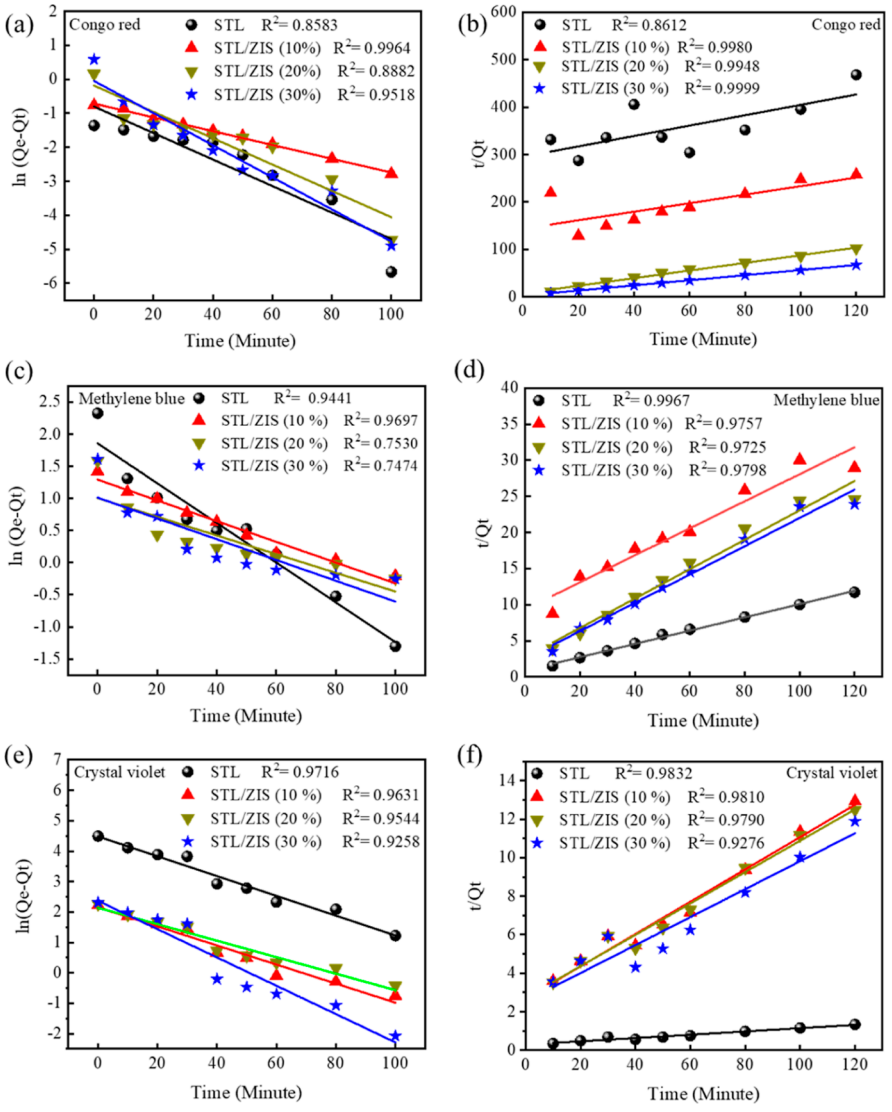


**Figure 10.** (a–f) Pseudo-first-order and second-order kinetics plot of CR, MB, and CV dyes.

## 5. PHOTOCATALYTIC STUDIES

In this photocatalytic experiment, one anionic dye, that is, CR, and two cationic dyes, that is, MB and CV, were used for investigating the photocatalytic degradation performance. For the aforementioned study, 100 mL of each dye solution (1 mg/100 mL) and 10, 20, and 50 mg of prepared samples (STL, STL/ZIS (10%), STL/ZIS (20%), and STL/ZIS (30%) were used to investigate the adsorption and photocatalysis behavior of the



https://doi.org/10.1021/acsomega.3c00955
ACS Omega 2023, 8, 17880−17890

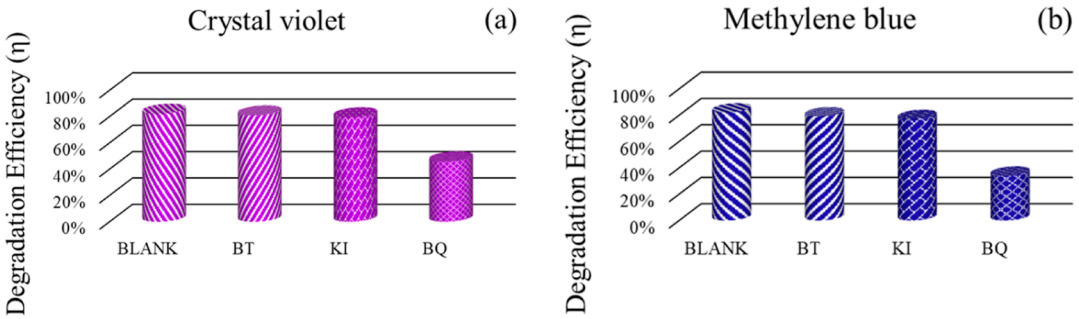


**Figure 11.** Scavenger study plot of (a) CV and (b) MB dyes using the STL/ZIS (30%) composite.

samples. For photocatalysis investigations, the experiment was carried out for 120 min under a light source (Xenon lamp), whereas adsorption tests were carried out for 60 min in the dark environment. The concentration of the dye was determined using UV−vis spectroscopy, after a fixed interval of time.

Figure 9a−f shows the $C/C_o$ versus time graph for CR, MB, and CV dye degradation in the absence and presence of a light source. $C$ denotes the absorption of dye after photocatalytic activity, when exposed for time $t$, and $C_o$ is the absorption of dye before exposure. It is quite interesting to note that in all the samples, dye degradation was very fast in the initial 30−40 min and then slows down at the end of the experiment. Figure 9g−i shows the degradation efficiency ($\eta$) of pure STL powder, STL/ZIS (10%), STL/ZIS (20%), and STL/ZIS (30%) composites for CR, CV, and MB dyes under dark and light source, respectively.

As illustrated in Figure 9g, STL perform poor degradation of the anionic dye (CR) due to the negative value of surface charge on STL. There is significant improvement on incorporation of ZIS, with degradation efficiency increasing from 9.58 to 19.37%, 49.57, and 77.58%, for STL/ZIS (10, 20, and 30%) sample, respectively. As illustrated in Figure 9h, the same trend was observed for degradation of CV dyes, degradation efficiency increasing from 65.30% (for pure STL powder) to 85.36% (for STL/ZIS 30). At the end of the experiment (120 min), the degradation efficiency of MB dye was highest (80.92%) for the STL/ZIS (30%) composite and lowest (91.28%) for STL adsorbent as shown in Figure 9i. The pristine STL sample shows intrinsically high degradation of MB dye; therefore, the improvement in degradation efficiency on incorporation of ZIS is not that significant, as in the case of CV dye. Based on the characterization results, STL/ZIS (30%) composite emerges as the optimized adsorbent, delivering best photocatalytic degradation efficiencies, in the case of both cationic and anionic dyes. As evident from the summarized reports, the novel STL/ZIS (30%) composite showed superior photocatalytic efficiency for both cationic as well as anionic dyes. All composites of STL powder were far efficient than pristine STL powder in degradation of cationic and anionic dyes.

Table 1 summarizes recent studies on the photocatalytic efficiency of various agricultural waste materials. The STL/ZIS composite was found to effectively degrade both anionic and cationic dyes, outperforming previous results.

**5.1. Adsorption Kinetic Study.** Adsorption kinetic study of anionic and cationic dyes onto the STL and STL/ZIS composite was studied using pseudo-first-order and pseudo-second-order eqs 3 and 4 as follows

$$\ln(Q_e - Q_t) = \ln(Q_e) - K_1 t \tag{3}$$

$$\frac{t}{Q_t} = \frac{1}{k_2 Q_e^2} + \frac{t}{Q_e} \tag{4}$$

where $Q_e$ and $Q_t$ are the amount of adsorbate/dye in the adsorbent (mg/g) at equilibrium time and instantaneous time ($t$) and calculated using eqs 5 and 6.

$$Q_t = (C_0 - C_t) \times \frac{V}{W} \tag{5}$$

$$Q_e = (C_0 - C_e) \times \frac{V}{W} \tag{6}$$

The first-order rate constant ($k_1$) is calculated from the slope of ln ($Q_e - Q_t$) versus time plot, whereas the second-order rate constant ($k_2$) is calculated using the $t/Q_t$ versus time plot. Figure 10a−f shows the results of the first-order and second-order kinetics models for CR, MB, and CV dye, respectively.

The pseudo-first-order process is a weak adsorption process that involved van der Waals interaction between the adsorbate and adsorbent, and in this process, no chemical interaction occurs between the adsorbate and adsorbent.[34] This process may happen in conditions when the solution concentration is low and when equilibrium is attained. The second-order process is the chemisorption process which involves the formation of relatively strong bonds with the surfaces.[36]

In contrast, the second order kinetics model fitted well into the adsorption process for both anionic and cationic dyes. This is also confirmed by the high value of the correlation coefficient ($R^2$), in the case of the second order kinetics model for both CR, CV, and MB dye, respectively. It suggested that the overall adsorption process is dominated by the chemisorption process and there are significant valence forces due to sharing or exchange of electrons between the photocatalyst sample and dye.

**5.2. Scavenger Study.** Scavenger experiment was performed to determine active species participate in photocatalytic mechanism for the degradation of dye. 1 mg of both CV and MB dye were dissolved in 100 mL of deionized water under the presence of different scavengers. Parabenzoquinone (BQ) serves as a scavenger for ($^{\bullet}O_2^-$), $t$-butanol ($t$-BuOH) for $^{\bullet}$OH, and potassium iodide (KI) for both hole and$^{\bullet}$OH radicals. Figure 11a−b depicts the influence of radicals on the dye degradation efficiency of the STL/ZIS composite for both CV and MB dyes. In Figure 11a, the degradation efficiency of the CV dye falls from an initial value of 82.04 to 80.83% on using t-BuOH, 79.38% on using KI, and 45.79% on using BQ. In the case of the MB dye, the degradation efficiency falls from 82.04 to 79.03% on using t-BuOH, 77% on using KI, and 34.00% using BQ, as shown in Figure 11b. The results clearly indicate



https://doi.org/10.1021/acsomega.3c00955
ACS Omega 2023, 8, 17880−17890

considerable influence of superoxide radical ($^{\bullet}O_2^-$) on a photocatalytic experiment for both CV and MB dyes.

**5.3. Photocatalytic Mechanism.** Figure 12 illustrates the mechanism of photocatalytic dye degradation in the STL/ZIS

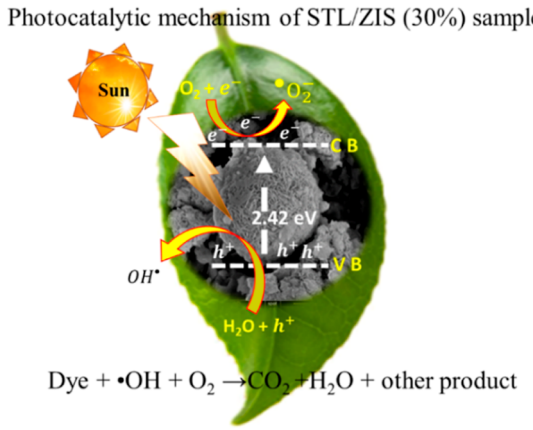


**Figure 12.** Schematic of photocatalytic mechanism of the STL/ZIS (30%) composite.

composite. During the photocatalytic process, when light with energy greater than the band gap of the photocatalyst sample is applied, an electron−hole pair is created. The holes in the conduction band react with the $H_2O$ molecule, producing the hydroxyl ($^{\bullet}OH$) radical and ($h^+$) ion as depicted in eqs 7−9.

$$STL/ZIS + hv \rightarrow STL/ZIS\ (e_{cb}^- + h_{vb}^+) \quad (7)$$

$$H_2O \rightarrow OH^- + H^+ \quad (8)$$

$$OH^- + h^+ \rightarrow {}^{\bullet}OH \quad (9)$$

Similarly, conduction band electron ($e^-$) reacts with oxygen radical ($O_2$) are produced superoxide radicle ($^{\bullet}O_2^-$). These radicals react with dye molecule and transform them into less harmful, nontoxic byproducts as given in eqs 10 and 11.

$$e_{cb}^- + O_2 \rightarrow {}^{\bullet}O_2^- \quad (10)$$

$$^{\bullet}O_2^- + \text{dye} \rightarrow \text{Non toxic byproduct} \quad (11)$$

**5.4. Recyclability Test.** Reusability of the STL/ZIS (10%) composite sample was investigated on the CV dye (1 mg/100 mL), using 10 mg of composite sample, for five cycles, as shown in Figure 13. In the first cycle, the composite induced 83.98% dye degradation. Next, the photocatalytic reduction solution was filtered, washed, and dried. The cleansed samples were again employed for the reduction of fresh CV solution and the

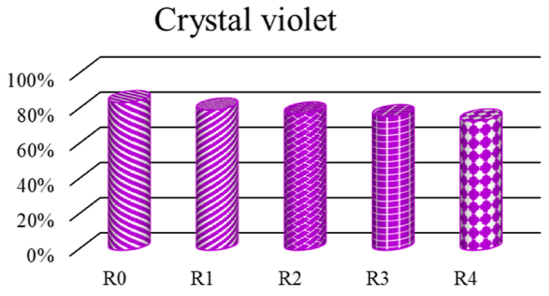


**Figure 13.** Recyclability plot of the STL/ZIS (10%) composite for the degradation of CV dye during five cycles.

photocatalysis efficiency was noted. The experiment was performed for five cycles and the photocatalysis efficiency slightly decreased from 83.98 to 73.54% after the fifth cycle. This slight change can be attributed to the photocatalyst waste after each cycle. The recyclability test clearly illustrates that the tea leaves composite (STL/ZIS) retained its dye degradation activity even after five cycles, thus emerging as excellent candidates for reusable adsorbent for dyes.

## 6. CONCLUSIONS

In this work, we report the synthesis of the STL/ZIS composite using an aqueous chemical solution method and performed in-depth investigation of comparative dye degradation activity of anionic dye (CR) and cationic dyes (MB and CV). XRD, FESEM, and HRTEM results were consistent in confirming the hexagonal phase of ZIS, with ZIS microspheres incorporated into the STL matrix. The element composition and oxidation state of the composite were confirmed by XPS.[66−72]

All composites STL/ZIS were found far efficient than the pristine STL powder sample, in degradation of cationic and anionic dyes and STL/ZIS (30%) sample shows the superior degradation efficiency ($\eta_{CR} \sim 77.18$, $\eta_{MB} \sim 85.36$, and $\eta_{CV} \sim 91.29$, in 120 min). Significant enhancement in photocatalytic degradation efficiency attributed to visible light response (as confirmed by tauc's plot), optimized surface charge (as observed from $\zeta$ potential), and low charge transfer resistance as observed from EIS study. Reaction kinetics was found to follow the second-order kinetic model, and the overall adsorption process is dominated by the chemisorption process. Photocatalysis mechanism along with trapping experiment was well explained. Reusability of the materials were also examined and samples demonstrated reusable properties up to five cycles. Spectacular improvement in dye-degradation efficiency of STL powder was demonstrated on ZIS incorporation. The study demonstrates that the STL/ZIS composite might be employed as an efficient, inexpensive, and eco-friendly photocatalyst for the dye degradation and wastewater treatment applications.

## AUTHOR INFORMATION


### Corresponding Author

**Manika Khanuja** − *Center for Nanoscience and Nanotechnology, Jamia Millia Islamia, New Delhi 110025, India;* orcid.org/0000-0001-8019-7621; Email: manikakhanuja@gmail.com

### Authors

**Mool Chand** − *Department of Physics, Hemvati Nandan Bahuguna Garhwal University (A Central University), Srinagar, Uttarakhand 246174, India*

**Swapnil Barthwal** − *Department of Energy Science and Engineering, Indian Institute of Technology (IIT) Delhi, New Delhi 110016, India*

**Arun Singh Rawat** − *Department of Physics, Hemvati Nandan Bahuguna Garhwal University (A Central University), Srinagar, Uttarakhand 246174, India*

**Seema Rawat** − *Department of Physics, Zakir Hussain Delhi College, New Delhi 110002, India*

Complete contact information is available at: https://pubs.acs.org/10.1021/acsomega.3c00955


### Notes

The authors declare no competing financial interest.



https://doi.org/10.1021/acsomega.3c00955
ACS Omega 2023, 8, 17880−17890

## ■ ACKNOWLEDGMENTS

The research work was funded by the Science and Engineering Research Board (SERB), India, under grant number ECR/2017/001222. The author, Mool Chand, expresses gratitude to the CSIR Delhi for providing fellowship support [09/386(0060)/2018-EMR-I].

## ■ REFERENCES

(1) Han, F.; Kambala, V. S. R.; Srinivasan, M.; Rajarathnam, D.; Naidu, R. Tailored Titanium Dioxide Photocatalysts for the Degradation of Organic Dyes in Wastewater Treatment: A Review. *Appl. Catal. A Gen.* **2009**, *359*, 25−40.
(2) Manju, S.; Sagar, N. Renewable Energy Integrated Desalination: A Sustainable Solution to Overcome Future Fresh-Water Scarcity in India. *Renew. Sustain. Energy Rev.* **2017**, *73*, 594−609.
(3) Cazzolla Gatti, R. Freshwater Biodiversity: A Review of Local and Global Threats. *Int. J. Environ. Stud.* **2016**, *73*, 887−904.
(4) Lellis, B.; Fávaro-Polonio, C. Z.; Pamphile, J. A.; Polonio, J. C. Effects of Textile Dyes on Health and the Environment and Bioremediation Potential of Living Organisms. *Biotechnol. Res. Innov.* **2019**, *3*, 275−290.
(5) Jamee, R.; Siddique, R. Biodegradation of Synthetic Dyes of Textile Effluent by Microorganisms: An Environmentally and Economically Sustainable Approach. *Eur. J. Microbiol. Immunol.* **2019**, *9*, 114−118.
(6) Drumond Chequer, F. M.; de Oliveira, G. A. R.; Anastacio Ferraz, E. R.; Carvalho, J.; Boldrin Zanoni, M. V.; de Oliveir, D. P. Textile Dyes: Dyeing Process and Environmental Impact. In *Eco-Friendly Textile Dyeing and Finishing*; InTech, 2013.
(7) Lee, K. M.; Lai, C. W.; Ngai, K. S.; Juan, J. C. Recent Developments of Zinc Oxide Based Photocatalyst in Water Treatment Technology: A Review. *Water Res* **2016**, *88*, 428−448.
(8) Ismail, M.; Akhtar, K.; Khan, M. I.; Kamal, T.; Khan, M. A.; M Asiri, A.; Seo, J.; Khan, S. B.; Khan, S. B. Pollution, Toxicity and Carcinogenicity of Organic Dyes and Their Catalytic Bio-Remediation. *Curr. Pharm. Des.* **2019**, *25*, 3645−3663.
(9) Kang, C.-W.; Kolya, H. Green Synthesis of Ag-Au Bimetallic Nanocomposites Using Waste Tea Leaves Extract for Degradation Congo Red and 4-Nitrophenol. *Sustainability* **2021**, *13*, 3318.
(10) Brown, M. A.; De Vito, S. C. Predicting Azo Dye Toxicity. *Crit. Rev. Environ. Sci. Technol.* **1993**, *23*, 249−324.
(11) Rawat, D.; Sharma, R. S.; Karmakar, S.; Arora, L. S.; Mishra, V. Ecotoxic Potential of a Presumably Non-Toxic Azo Dye. *Ecotoxicol. Environ. Saf.* **2018**, *148*, 528−537.
(12) Massey, A. T.; Gusain, R.; Kumari, S.; Khatri, O. P. Hierarchical Microspheres of $MoS_2$ Nanosheets: Efficient and Regenerative Adsorbent for Removal of Water-Soluble Dyes. *Ind. Eng. Chem. Res.* **2016**, *55*, 7124−7131.
(13) Han, S.; Liu, K.; Hu, L.; Teng, F.; Yu, P.; Zhu, Y. Superior Adsorption and Regenerable Dye Adsorbent Based on Flower-Like Molybdenum Disulfide Nanostructure. *Sci. Rep.* **2017**, *7*, 43599.
(14) Lazar, M.; Varghese, S.; Nair, S. Photocatalytic Water Treatment by Titanium Dioxide: Recent Updates. *Catalysts* **2012**, *2*, 572−601.
(15) Serpone, N.; Emeline, A. V. Semiconductor Photocatalysis — Past, Present, and Future Outlook. *J. Phys. Chem. Lett.* **2012**, *3*, 673−677.
(16) Kamat, P. V.; Jin, S. Semiconductor Photocatalysis: " Tell Us the Complete Story. *ACS Energy Lett* **2018**, *3*, 622−623.
(17) Kumar, A.; Mittal, H.; Nagar, R.; Khanuja, M. The Synergistic Effect of Acid-Etched g-$C_3N_4$ Nanosheets and Polyaniline Nanofibers for the Adsorption and Photocatalytic Degradation of Textile Dyes: A Study of Charge Transfer Mechanism and Intermediate Products. *Mater. Adv.* **2022**, *3*, 5325−5336.
(18) Mittal, H.; Khanuja, M. Nanosheets- and Nanourchins-like Nanostructures of $MoSe_2$ for Photocatalytic Water Purification: Kinetics and Reusability Study. *Environ. Sci. Pollut. Res.* **2020**, *27*, 23477−23489.
(19) Ashraf, W.; Khan, A.; Bansal, S.; Khanuja, M. Mechanical ball milling: A sustainable route to induce structural transformations in tungsten disulfide for its photocatalytic applications. *Physica E: Low-dimensional Systems and Nanostructures* **2022**, *140*, 115152.
(20) Fatima, T.; Husain, S.; Khanuja, M. Superior Photocatalytic and Electrochemical Activity of Novel $WS_2$/PANI Nanocomposite for the Degradation and Detection of Pollutants: Antibiotic, Heavy Metal Ions, and Dyes. *Chem. Eng. J. Adv.* **2022**, *12*, 100373.
(21) Hameed, B. H. Spent Tea Leaves: A New Non-Conventional and Low-Cost Adsorbent for Removal of Basic Dye from Aqueous Solutions. *J. Hazard. Mater.* **2009**, *161*, 753−759.
(22) Hayat, K.; Iqbal, H.; Malik, U.; Bilal, U.; Mushtaq, S. Tea and Its Consumption: Benefits and Risks. *Crit. Rev. Food Sci. Nutr.* **2015**, *55*, 939−954.
(23) Auta, M.; Hameed, B. H. Preparation of Waste Tea Activated Carbon Using Potassium Acetate as an Activating Agent for Adsorption of Acid Blue 25 Dye. *Chem. Eng. J.* **2011**, *171*, 502−509.
(24) El-Azazy, M.; El-Shafie, A. S.; Al-Shaikh Yousef, B. Green Tea Waste as an Efficient Adsorbent for Methylene Blue: Structuring of a Novel Adsorbent Using Full Factorial Design. *Molecules* **2021**, *26*, 6138.
(25) Hussain, S.; Anjali, K. P.; Hassan, S. T.; Dwivedi, P. B. Waste Tea as a Novel Adsorbent: A Review. *Appl. Water Sci.* **2018**, *8*, 165.
(26) Amarasinghe, B. M. W. P. K.; Williams, R. A. Tea Waste as a Low Cost Adsorbent for the Removal of Cu and Pb from Wastewater. *Chem. Eng. J.* **2007**, *132*, 299−309.
(27) Çelebi, H.; Gök, G.; Gök, O. Adsorption Capability of Brewed Tea Waste in Waters Containing Toxic Lead(II), Cadmium (II), Nickel (II), and Zinc(II) Heavy Metal Ions. *Sci. Rep.* **2020**, *10*, 17570.
(28) Dutta, S.; Gupta, B.; Srivastava, S. K.; Gupta, A. K. Recent Advances on the Removal of Dyes from Wastewater Using Various Adsorbents: A Critical Review. *Mater. Adv.* **2021**, *2*, 4497−4531.
(29) Wang, T.; Qu, G.; Pei, S.; Liang, D.; Hu, S. Research on Dye Wastewater Decoloration by Pulse Discharge Plasma Combined with Charcoal Derived from Spent Tea Leaves. *Environ. Sci. Pollut. Res.* **2016**, *23*, 13448−13457.
(30) Lin, D.; Wu, F.; Hu, Y.; Zhang, T.; Liu, C.; Hu, Q.; Hu, Y.; Xue, Z.; Han, H.; Ko, T.-H. Adsorption of Dye by Waste Black Tea Powder: Parameters, Kinetic, Equilibrium, and Thermodynamic Studies. *J. Chem.* **2020**, *2020*, 1−13.
(31) Wong, S.; Tumari, H. H.; Ngadi, N.; Mohamed, N. B.; Hassan, O.; Mat, R.; Saidina Amin, N. A. Adsorption of Anionic Dyes on Spent Tea Leaves Modified with Polyethyleneimine (PEI-STL). *J. Clean. Prod.* **2019**, *206*, 394−406.
(32) Hashemian, S.; Ardakani, M. K.; Salehifar, H. Kinetics and Thermodynamics of Adsorption Methylene Blue onto Tea Waste/CuFe2$O_4$ Composite. *Am. J. Anal. Chem.* **2013**, *04*, 1−7.
(33) Bo, L.; Kiriarachchi, H. D.; Bobb, J. A.; Ibrahim, A. A.; El-shall, M. S. Preparation, Activity, and Mechanism of ZnIn2S4-Based Catalysts for Photocatalytic Degradation of Atrazine in Aqueous Solution. *J. Water Process Eng.* **2020**, *36*, 101334.
(34) Song, Y.; Zhang, J.; Dong, X.; Li, H. A Review and Recent Developments in Full-Spectrum Photocatalysis Using ZnIn 2 S 4 -Based Photocatalysts. *Energy Technol* **2021**, *9*, 2100033.
(35) Yang, R.; Mei, L.; Fan, Y.; Zhang, Q.; Zhu, R.; Amal, R.; Yin, Z.; Zeng, Z. $ZnIn_2S_4$-Based Photocatalysts for Energy and Environmental Applications. *Small Methods* **2021**, *5*, 2100887.
(36) Imran, M.; Ashraf, W.; Hafiz, A. K.; Khanuja, M. Synthesis and Performance Analysis of Photocatalytic Activity of $ZnIn_2S_4$ Microspheres Synthesized Using a Low-Temperature Method. *ACS Omega* **2022**, *7*, 22987−22996.
(37) Chachvalvutikul, A.; Pudkon, W.; Luangwanta, T.; Thongtem, T.; Thongtem, S.; Kittiwachana, S.; Kaowphong, S. Enhanced Photocatalytic Degradation of Methylene Blue by a Direct Z-Scheme $Bi_2S_3$/$ZnIn_2S_4$ Photocatalyst. *Mater. Res. Bull.* **2019**, *111*, 53−60.
(38) Cai, H. m.; Chen, G. j.; Peng, C. y.; Zhang, Z. z.; Dong, Y. y.; Shang, G. z.; Zhu, X. h.; Gao, H. j.; Wan, X. c. Removal of Fluoride from Drinking Water Using Tea Waste Loaded with Al/Fe Oxides: A Novel, Safe and Efficient Biosorbent. *Appl. Surf. Sci.* **2015**, *328*, 34−44.


https://doi.org/10.1021/acsomega.3c00955
*ACS Omega* 2023, 8, 17880−17890

(39) Chand, M.; Rawat, A. S.; Khanuja, M.; Rawat, S.; Ranwa, M. Synthesis of Marigold-like $ZnIn_2S_4$ Microspheres at Low-Temperature. *Mater. Today Proc.* **2022**, *49*, 2297−2300.
(40) Cai, J. x.; Wang, Y. f.; Xi, X. g.; Li, H.; Wei, X. l. Using FTIR Spectra and Pattern Recognition for Discrimination of Tea Varieties. *Int. J. Biol. Macromol.* **2015**, *78*, 439−446.
(41) Duan, J.; Reddy, K. O.; Ashok, B.; Cai, J.; Zhang, L.; Rajulu, A. V. Effects of Spent Tea Leaf Powder on the Properties and Functions of Cellulose Green Composite Films. *J. Environ. Chem. Eng.* **2016**, *4*, 440−448.
(42) Unger, W. K.; Farnworth, B.; Irwin, J. C.; Pink, H. Raman and Infrared Spectra of $CdIn_2S_4$ and $ZnIn_2S_4$. *Solid State Commun* **1978**, *25*, 913−915.
(43) Li, Y.; Zhang, K.; Peng, S.; Lu, G.; Li, S. Photocatalytic Hydrogen Generation in the Presence of Ethanolamines over $Pt/ZnIn_2S_4$ under Visible Light Irradiation. *J. Mol. Catal. A Chem.* **2012**, *363*−*364*, 354−361.
(44) Enders, A. A.; North, N. M.; Fensore, C. M.; Velez-Alvarez, J.; Allen, H. C. Functional Group Identification for FTIR Spectra Using Image-Based Machine Learning Models. *Anal. Chem.* **2021**, *93*, 9711−9718.
(45) Tu, X.; Lu, J.; Li, M.; Su, Y.; Yin, G.; He, D. Hierarchically $ZnIn_2S_4$ Nanosheet-Constructed Microwire Arrays: Template-Free Synthesis and Excellent Photocatalytic Performances. *Nanoscale* **2018**, *10*, 4735−4744.
(46) Zhang, G.; Zhu, X.; Chen, D.; Li, N.; Xu, Q.; Li, H.; He, J.; Xu, H.; Lu, J. Hierarchical Z -Scheme g-$C_3N_4$/Au/$ZnIn_2S_4$ Photocatalyst for Highly Enhanced Visible-Light Photocatalytic Nitric Oxide Removal and Carbon Dioxide Conversion. *Environ. Sci. Nano* **2020**, *7*, 676−687.
(47) Chai, B.; Peng, T.; Zeng, P.; Zhang, X. Preparation of a MWCNTs/$ZnIn_2S_4$ Composite and Its Enhanced Photocatalytic Hydrogen Production under Visible-Light Irradiation. *Dalt. Trans.* **2012**, *41*, 1179−1186.
(48) Ahmad, R.; Kumar, R. Conducting Polyaniline/Iron Oxide Composite: A Novel Adsorbent for the Removal of Amido Black 10B. *J. Chem. Eng. Data* **2010**, *55*, 3489−3493.
(49) Kumar, R.; Ansari, S. A.; Barakat, M. A.; Aljaafari, A.; Cho, M. H. A Polyaniline@$MoS_2$ -Based Organic−Inorganic Nanohybrid for the Removal of Congo Red: Adsorption Kinetic, Thermodynamic and Isotherm Studies. *New J. Chem.* **2018**, *42*, 18802−18809.
(50) Arivoli, S.; Thenkuzhali, M.; Prasath, M. Adsorption of Rhodamine B by Acid Activated Carbon-Kinetic, Thermodynamic and Equilibrium Studies. *Orbital Electron. J. Chem.* **2009**, *1*. DOI: 10.17807/orbital.v1i2.24
(51) Reddy, M. C. Removal of Direct Dye from Aqueous Solutions with a Novel Adsorbent Made from Tamarind Fruit Shell, an Agricultural Solid Waste. *J. Sci. Ind. Res. (India).* **2006**, *65*. DOI: 10.1016/j.dyepig.2006.06.009.
(52) Bhattacharyya, K. G.; Sharma, A. Azadirachta Indica Leaf Powder as an Effective Biosorbent for Dyes: A Case Study with Aqueous Congo Red Solutions. *J. Environ. Manage.* **2004**, *71*, 217−229.
(53) Abdelwahab, O.; Nemr, A.; Sikaily, A.; Khaled, A. Use of rice husk for adsorption of direct dyes from aqueous solution: A case study of direct F. Scarlet. *Egypt. J. Aquat. Res.* **2005**, *31*.
(54) Srivastava, R.; Rupainwar, D. C. A Comparative Evaluation for Adsorption of Dye on Neem Bark and Mango Bark Powder. *Indian J. Chem. Technol.* **2011**, *18*, 67−75.
(55) Hassanein, T. F.; Koumanova, B. Evaluation of ad-sorption potential of the agricultural waste wheat straw for Basic Yellow 21. *J. Univ. Chem. Technol. Metall.* **2010**, *45*, 407−414.
(56) Tan, L. S.; Jain, K.; Rozaini, C. A. Adsorption of textile dye from aqueous solution on pretreated mangrove bark, an agricultural waste: equilibrium and kinetic studies. *J. Appl. Sci. Environ. Sanit.* **2010**, *5*, 283−293.
(57) Ncibi, M. C.; Mahjoub, B.; Seffen, M. Adsorptive Removal of Textile Reactive Dye Using Posidonia Oceanica (L.) Fibrous Biomass. *Int. J. Environ. Sci. Technol.* **2007**, *4*, 433−440.
(58) Patil, S.; Renukdas, S.; Patel, N. Removal of Methylene Blue, a Basic Dye from Aqueous Solutions by Adsorption Using Teak Tree (Tectona Grandis) Bark Powder. *Remov. methylene blue, a basic Dye from aqueous Solut. by Adsorpt. using teak tree ( Tectona Gd. bark powder* **2011**, *1*, 711−726.
(59) Sharma, Y.; Singh, B. Fast Removal of Malachite Green by Adsorption on Rice Husk Activated Carbon. *Open Environ. Pollut. Toxicol. J.* **2009**, *1*, 74−78.
(60) Chandrasekhar, S.; Pramada, P. N. Rice Husk Ash as an Adsorbent for Methylene Blue—Effect of Ashing Temperature. *Adsorption* **2006**, *12*, 27−43.
(61) Singh, S.; Parveen, N.; Gupta, H. Adsorptive Decontamination of Rhodamine-B from Water Using Banana Peel Powder: A Biosorbent. *Environ. Technol. Innov.* **2018**, *12*, 189−195.
(62) Vigneshwaran, S.; Sirajudheen, P.; Karthikeyan, P.; Meenakshi, S. Fabrication of Sulfur-Doped Biochar Derived from Tapioca Peel Waste with Superior Adsorption Performance for the Removal of Malachite Green and Rhodamine B Dyes. *Surfaces and Interfaces* **2021**, *23*, 100920.
(63) Saigl, Z. M.; Ahmed, A. M. Separation of Rhodamine b Dye from Aqueous Media Using Natural Pomegranate Peels. *Indones. J. Chem.* **2020**, *21*, 212−224.
(64) Zuorro, A.; Lavecchia, R.; Medici, F.; Piga, L. Spent Tea Leaves as a Potential Low-Cost Adsorbent for the Removal of Azo Dyes from Wastewater. *Chem. Eng. Trans.* **2013**, *32*, 19−24.
(65) Dakhil, I. H. Adsorption of Methylene Blue Dye from Wastewater By Spent Tea Leaves. *J. Kerbala Univ.* **2013**, *11*, 5−14.
(66) Jia, P.; Tan, H.; Liu, K.; Gao, W. S. Synthesis, characterization and photocatalytic property of novel ZnO/bone char composite. *Mater. Res. Bull.* **2018**, *102*, 45−50.
(67) Sinha, T.; Ahmaruzzaman, M. Green Synthesis of Copper Nanoparticles for the Efficient Removal (Degradation) of Dye from Aqueous Phase. *Environ. Sci. Pollut. Res.* **2015**, *22*, 20092−20100.
(68) Hisaindee, S.; Meetani, M. A.; Rauf, M. A. Application of LC-MS to the Analysis of Advanced Oxidation Process (AOP) Degradation of Dye Products and Reaction Mechanisms. *TrAC Trends Anal. Chem.* **2013**, *49*, 31−44.
(69) Rauf, M. A.; Meetani, M. A.; Khaleel, A.; Ahmed, A. Photocatalytic Degradation of Methylene Blue Using a Mixed Catalyst and Product Analysis by LC/MS. *Chem. Eng. J.* **2010**, *157*, 373−378.
(70) Prabakaran, E.; Pillay, K. Synthesis of N-Doped ZnO Nanoparticles with Cabbage Morphology as a Catalyst for the Efficient Photocatalytic Degradation of Methylene Blue under UV and Visible Light. *RSC Adv* **2019**, *9*, 7509−7535.
(71) Mrunal, V. K.; Vishnu, A. K.; Momin, N.; Manjanna, J. $Cu_2O$ Nanoparticles for Adsorption and Photocatalytic Degradation of Methylene Blue Dye from Aqueous Medium. *Environ. Nanotechnology, Monit. Manag.* **2019**, *12*, 100265.
(72) Sood, S.; Umar, A.; Mehta, S. K.; Kansal, S. K. Highly Effective Fe-Doped $TiO_2$ Nanoparticles Photocatalysts for Visible-Light Driven Photocatalytic Degradation of Toxic Organic Compounds. *J. Colloid Interface Sci.* **2015**, *450*, 213−223.


https://doi.org/10.1021/acsomega.3c00955
*ACS Omega* 2023, 8, 17880−17890